DOI:10.1093/jnci/djs336
Advance Access publication on August 21, 2012.

ARTICLE

Targeting Carcinoma-Associated Fibroblasts Within the Tumor Stroma With a Fibroblast Activation Protein-Activated Prodrug

W. Nathaniel Brennen, D. Marc Rosen, Hao Wang, John T. Isaacs, Samuel R. Denmeade

Manuscript received November 10, 2011; revised June 26, 2012; accepted June 28, 2012.

Correspondence to: Samuel R. Denmeade, MD, Department of Oncology, The Johns Hopkins University School of Medicine, Cancer Research Building I, Rm 1M43, 1650 Orleans St, Baltimore, MD 21231 (e-mail: denmesa@jhmi.edu).

Background Fibroblasts undergo a morphological transformation to a reactive phenotype in the tumor microenvironment characterized by the expression of proteins such as fibroblast activation protein (FAP), a post-prolyl endopeptidase with expression largely restricted to carcinoma-associated fibroblasts. Thapsigargin (TG) is a highly toxic natural plant product that triggers a rise in intracellular calcium levels and apoptosis. FAP is therefore a provocative target for the activation of prodrugs consisting of a FAP-specific peptide coupled to a potent cytotoxic analog of TG.

Methods The efficacy of FAP-activated peptidyl-TG prodrugs was tested in vitro in cell proliferation assays and effects on intracellular calcium in human cancer cell lines. The effects of FAP-activated prodrugs on tumor growth and host toxicity were tested in Balb-C nude MCF-7 and LNCaP xenograft mice (n = 9–11 per group). *P* values were calculated using permutation tests based on 50 000 permutations. Mixed effects models were used to account for correlations among replicate measures. All statistical tests were two-sided.

Results FAP-activated prodrugs killed human cancer cells at low nanomolar concentrations (MCF-7 cells: IC_{50} = 3.5 nM). Amino acid-12ADT analogs from FAP-cleaved prodrugs, but not uncleaved prodrugs, produced a rapid rise in intracellular calcium within minutes of exposure. Immunohistochemical analysis of xenografts exposed to FAP-prodrugs documented stromal-selective cell death of fibroblasts, pericytes, and endothelial cells of sufficient magnitude to inhibit growth of MCF-7 and LNCaP xenografts with minimal systemic toxicity, whereas non-FAP cleavable prodrugs were inactive. MCF-7 and LNCaP xenografts treated with a FAP-activated prodrug had maximal treated-to-control tumor volume ratios of 0.36 (treated: mean = 0.206 mm^3, 95% CI = 0.068 to 0.344 mm^3; control: mean = 0.580 mm^3, 95% CI = 0.267 to 0.893 mm^3) and 0.24 (treated: mean = 0.131 mm^3, 95% CI = 0.09 to 0.180 mm^3; control: mean = 0.543 mm^3, 95% CI = 0.173 to 0.913mm^3), respectively, on day 21 after therapy.

Conclusions This study validates the proteolytic activity of FAP as a target for the activation of a systemically delivered cytotoxic prodrug and demonstrates that targeted killing of cells within the stromal compartment of the tumor microenvironment can produce a therapeutic response.

J Natl Cancer Inst 2012;104:1320–1334

The tumor stroma constitutes a substantial portion of the mass of many malignancies, including more than 90% of cancers characterized by a desmoplastic reaction (1–3). Tumor cells depend upon the stroma for growth and survival signals, in addition to the nutritional support necessary for tumor maintenance and expansion. When associated with a transformed epithelium, the tumor stroma becomes "activated" (4). Fibroblasts, in particular, consistently undergo changes in morphology and expression profiles when present in the tumor microenvironment (5). These carcinoma-associated fibroblasts (CAFs) produce growth factors that promote tumor growth, angiogenesis, and the recruitment of protumorigenic inflammatory cells (6,7). CAFs can also affect the sensitivity of malignant cells to chemotherapy or radiotherapy (8,9). Furthermore, fibroblast activation protein-alpha (FAP)-positive cells within the stroma may also alter the antitumor immune response (10). Additionally, CAFs alter the extracellular matrix through the production of proteases such as FAP (11–13). FAP is a type II integral membrane serine protease of the dipeptidyl peptidase IV family, which is characterized by post-prolyl cleavage specificity (14,15). However, FAP is unique in this family of enzymes because, in addition to its dipeptidase activity, it also possesses a collagen type I-restricted gelatinase activity (11,16–18). FAP is selectively expressed on the plasma membrane of reactive fibroblasts and pericytes, in the stroma surrounding most epithelial cancers with minimal to no expression by malignant epithelial cells (12,19–21). These FAP-expressing cells may represent or be derived from

mesenchymal stem cells that have trafficked to the tumor from bone marrow or other sites (22). Although FAP-positive cells are also observed during wound healing, embryogenesis, and in areas of chronic inflammation and fibrosis (23–26); normal, healthy adult tissues have almost no detectable FAP expression (12,19–21).

We developed a therapeutic strategy that exploits FAP's relative tumor-restricted expression and unique proteolytic activity to activate a peptide-based cytotoxic prodrug within the tumor microenvironment. This approach specifically targets the FAP-expressing CAFs. However, prodrug activation in the extracellular space could also result in the death of non-FAP expressing cell types, such as endothelial cells, due to a bystander effect. Directing therapy at FAP-expressing CAFs within the reactive stroma offers the advantages of providing a more genetically stable target (27) and represents a potential pantumor therapeutic approach because of the common microenvironmental alterations that occur in many different solid tumors (11,28). Here we report the generation of FAP-activated prodrugs that have been characterized for in vitro and in vivo antitumor activity against human breast and prostate cancer models.

Materials and Methods

Reagents

Dulbecco's modified Eagle medium (DMEM), Roswell Park Memorial Institute (RPMI) 1640 medium, RPMI 1640 (phenol-free), L-glutamine, penicillin-streptomycin, fetal bovine serum (FBS)-heat inactivated, and bovine serum were all obtained from Invitrogen (Carlsbad, CA); FBS from Thermo Scientific (Waltham, MA); polyclonal rabbit anti-mouse FAP polyclonal antibody was provided by Dr JD Cheng (Fox Chase Cancer Center); Monoclonal Rat anti-Mouse Ki-67 Antigen (Clone TEC-3), Monoclonal Mouse anti-Human Desmin, and Monoclonal Mouse anti-Human Smooth Muscle Actin (Clone 1A4) were from Dako (Carpinteria, CA); Monoclonal Mouse anti-Vimentin (Clone LN-6) from Sigma-Aldrich (St Louis, MO); Polyclonal Rabbit anti-Mouse Vimentin from Cell Signaling (Danvers, MA); Polyclonal Rabbit anti-NG2 Chondroitin Sulfate Proteoglycan from Millipore (Billerica, MA); Polyclonal Rat anti-Mouse CD31 (Clone MEC 13.3) from BD Biosciences (Franklin Lakes, NJ); Alexa Fluor 488 Goat anti-Rat IgG, Alexa Fluor 568 Goat anti-Mouse IgG, Alexa Fluor 488 Goat anti-Rabbit, and Alexa Fluor 546 Goat anti-Rabbit were all obtained from Santa Cruz Biotechnology (Santa Cruz, CA). Synthesis of acetylated-gly-proline boronic acid (boro-Pro) (AcGbP) was performed as described previously (29,30). Boc-protected 12-aminododecanoyl thapsigargin (Boc-12ADT) was provided by Dr Søeren Brogger Christensen, University of Copenhagen, Denmark. 12ADT-conjugated peptide prodrugs were produced by coupling solid phase synthesized peptide to 12ADT, and this was performed by California Peptide Research (Napa, CA) according to previously described methods (31). FAP was recombinantly expressed using Schneider's S2 cells and purified from the culture supernatant after induction with 500 μM $CuSO_4$ using Ni-NTA resin (Qiagen, Valencia, CA) as previously described (17).

Cell Lines

Human LNCaP prostate cancer, TSU bladder cancer, and MCF-7 breast cancer cell lines were obtained from ATCC (Manassas, VA). LNCaP and TSU cells were grown as a monolayer in RPMI 1640 supplemented with 10% FBS, 1% L-glutamine, and 1% Pen/Strep at 37°C in a humidified incubator with 5% CO_2. MCF-7 cells were grown in an analogous manner using DMEM medium. Schneider's S2 (Invitrogen, Carlsbad, CA) cells were grown as a suspension culture at room temperature in Drosophila expression system medium (Invitrogen) supplemented with heat-inactivated FBS.

Generation of Prodrugs

Prodrugs were synthesized by California Peptide (Napa, CA) according to previously published protocols (31). Three FAP-activated prodrugs were generated: ASGPAGPA-A12ADT, DSGETGP-A12ADT, and ERGETGP-S12ADT (Figure 1, A). In addition, two non-FAP cleavable prodrug controls were generated, one in which the peptide sequence was scrambled (PETGRSG-E12ADT) and one in which the P1-proline at the FAP cleavage site was converted to the D-isomer (ERGETGp-S12ADT). The amino termini were protected with a morpholino (μ) cap.

FAP-Mediated Hydrolysis of Prodrugs Ex Vivo

All prodrugs (three FAP-activated and two noncleavable controls) (1 μM final concentration) were added to FAP buffer ± 10 μM AcGbP or DMEM media ± 10% FBS. All samples contained 10% DMSO and were incubated at 37°C for 24 hours in a shaking incubator with or without 200 nM FAP. Prodrug hydrolysis was monitored by high-pressure liquid chromatography/quadripole mass spectroscopy (LCMS; PE Sciex API 3000, Applied Biosystems, Carlsbad, CA) detection of the active form of each drug (A-, S-, E-12ADT) at 0 and 24 hours in a single experiment.

Measurement of Intracellular Ca^{2+} Concentration

Ratiometric measurement of intracellular calcium levels was performed using fura2-AM loaded TSU cells in a cuvette fluorometer (Photon Technology International, Birmingham, NJ) according to previously described methods (32). The fluorescence ratio was monitored at an emission wavelength of 510 nm following excitation at 340 and 380 nm over 20 min. Intracellular calcium was determined according to the following formula: $[Ca^{2+}] = K_d Q[(R - R_{min})/(R_{max} - R)]$, where R corresponds to the peak fluorescence ratio at 340 nm/380 nm, Q is the F_{min} to F_{max} ratio at 380 nm, and the K_d is equal to 150 nM. R_{max} was determined by lysing cells with 0.5% Triton X-100 and R_{min} by chelating all free calcium with addition of 5 mM EGTA. Pro- and active forms of the drug were added to final concentrations of 50, 1000, or 5000 nM after baseline readings were obtained. FAP was added at a final concentration of 200 nM when indicated, and changes in fluorescence ratios were monitored over 1 hour and then converted to intracellular calcium levels. Three to six replicates were performed per concentration per compound.

Efficacy of Prodrugs In Vitro

Cell proliferation assays (3-[4,5-dimethylthiazolyl-2]-2,5-diph enyltetrazolium bromide, MTT) were performed according to the manufacturer's instructions (Promega, Madison, WI) after cells (MCF-7, WPMY-1, CAS-23, or NAS-23) were exposed to either the prodrugs (ASGPAGP-A12ADT, DSGETGP-A12ADT, ERGETGP-S12ADT,ERGETGp-S12ADT,PETGRSG-E12ADT) or the active drugs (A12ADT, S12ADT, E12ADT, or 12ADT) for 0,

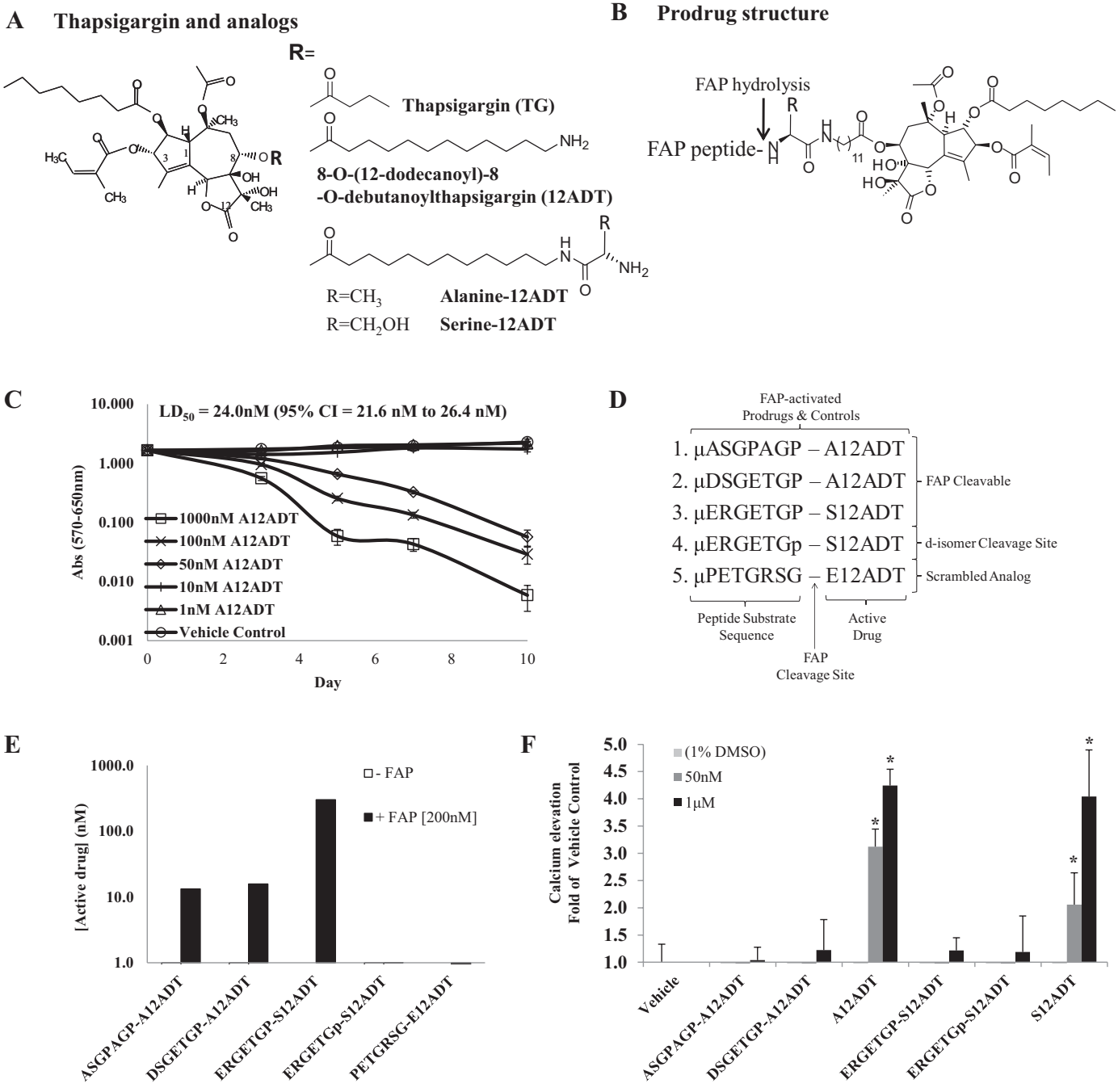

Figure 1. Design and in vitro characterization of FAP-activated prodrugs. **A**) Structure of the potent natural plant product thapsigargin (TG) and its analogs, which are used as the cytotoxic "warhead" in FAP-activated prodrugs. **B**) Diagram of FAP-activated prodrug structure. Prodrugs consist of a peptide carrier containing a FAP-selective cleavage site coupled to a TG analog via a linker. **C**) The A12ADT amino acid-containing TG analog is as toxic against quiescent, nonproliferating fibroblasts as it is against those in the exponential growth phase. Results are the means of one independent experiment with seven replicates. Statistically significant $P < .05$, determined using permutation tests in a mixed effects model. **D**) Design of FAP-activated prodrugs and controls. Peptide sequences are based upon the substrate specificity of FAP as determined from a human collagen I-derived gelatin cleavage map (17) and were coupled to a thapsigargin analog, 8-*O*-(12-aminododecanoyl)-8-*O*-debutanoyl thapsigargin (12ADT). Two prodrug analog controls were also designed based on our lead sequence, one with the P1-Pro in the cleavage position converted to a D-isomer (represented by a "p") and one with the amino acid sequence scrambled. **E**) FAP enzymatic activity can hydrolyze the FAP-activated prodrugs in vitro, but not the D-isomer and scrambled analog controls. **F**) The TSU human bladder cancer cell line was treated with increasing concentrations of the prodrugs or the active drug, and the effect on intracellular [Ca^{2+}] was measured using the Fura-2, AM cell-permeable dye. The S- and A12ADT TG analogs (ie, the active forms of the prodrug) are able to induce a rapid rise in [Ca^{2+}] at concentrations of 50 nM, whereas the full-length inactive prodrugs do not cause this rise in cytosolic [Ca^{2+}] even at concentrations 20-fold higher, 1 μM. Fifty nanomolar concentration only shown for active forms of the prodrug. **Error bars** represent 95% CI. Results are the means of three to six replicates per concentration per compound. **Asterisks** indicate statistically significant $P < .05$, determined using permutation test to compare means. (Note: mean of the replicates was used in the analysis.) TG = thapsigargin; FAP = fibroblast activation protein α; LD_{50} = lethal dose, 50%; CI = confidence interval.

3, 5, and 7 days (31). Absorbance was read at 570 nm with a correction wavelength of 650 nm on a SpectraMax Plus (Molecular Devices, Sunnyvale, CA). Mean absorbance was calculated from a single experiment with seven replicates per concentration and reported with 95% confidence intervals (CI). Concentrations that inhibited growth by 50% (IC_{50}) were calculated as the concentration at which absorbance equaled 50% of the vehicle control after a 7-day exposure. Clonal survival assays were performed as previously described (33).

FAP Enzymatic Activity in Plasma, Serum, and Tumor Homogenates Ex Vivo

FAP enzymatic activity was measured in plasma, serum, and tumor homogenates by cleavage of fluorescence-quenched peptide substrates as described previously (17). MCF-7 tumors were homogenized in 2X cOmplete, EDTA-free protease inhibitor (Roche, Basel, Switzerland). For inhibition studies, tumor homogenate was preincubated with AcGbP for 30 minutes at 37°C in a shaking incubator before addition of substrate.

FAP enzymatic activity in plasma and serum was measured using the substrate MCa-ASGPAGPA-Dnp (20 μM) at increased inhibitor concentration to 200 μM. Mouse and rat plasma/serum were collected by intracardiac puncture of fully anesthetized animals. Human plasma/serum was from discarded clinical specimens. Horse and chicken sera were obtained from Vector Laboratories (Burlingame, CA). Rates of hydrolysis were calculated as the slope (k) of fluorescence output from substrate cleavage over time (k [RFU/min]).

Immunohistochemistry

Excised tumors were flash-frozen in liquid nitrogen. Sections (4 μM) were cut on a Shandon Cryotome E (Thermo Scientific) by the Johns Hopkins Oncology Histology Core. Slides were washed twice in PBS for 5 minutes and fixed in cold 100% acetone at –20°C for 20 minutes. Three additional washes in PBS for 5 minutes per wash were followed by a 30-minute incubation with 0.3% H_2O_2 diluted in methanol to block endogenous peroxidase activity. After washing, slides were blocked in PBS plus 5% goat serum (Vector Labs). Slides were incubated with a rabbit anti-mouse FAP polyclonal antibody (kindly provided by JD Cheng) diluted 1:1000 (25 μg) in PBS plus 1% FBS or normal rabbit IgG (25 μg) (Santa Cruz Biotechnology, Santa Cruz, CA) at 4°C for 2 hours followed by three washes in PBS plus 1% FBS for 5 minutes per wash. Slides were then incubated with biotinylated-goat-anti-rabbit IgG (Vector Labs) diluted 1:1000 in PBS plus 1% FBS for 1 hour at room temperature and then washed three times. Slides were incubated with the VectaStain ABC complex (Vector Labs) per manufacturer's instructions and then stained with Mayer's hematoxylin stain (Dako, Carpinteria, CA).

For immunofluorescent assays, untreated controls and prodrug-treated animals were perfused with 2% paraformaldehyde 24 hours after their third consecutive daily 0.1-mL IV injection of a 1 mM prodrug. Cardiac perfusion was performed as previously described (34,35). Briefly, following lethal anesthetization of mice with ketamine/xylazine, the chest cavity was rapidly opened and a blunt needle was inserted into the heart through an incision in the left ventricle. The mice were initially perfused with PBS at approximately 120 mm Hg until the blood was cleared from circulation and then perfused with 2% paraformaldehyde in PBS for 5 minutes. Tumors were removed and fixed for an additional hour in 2% paraformaldehyde at room temperature before soaking in a 30% sucrose solution for 3–5 days. Subsequently, tumors were embedded in tissue freezing medium (Triangle Biomedical Sciences, Durham, NC), and 4 μM sections were cut on a Shandon Cryotome E (Thermo Scientific) by the Johns Hopkins Oncology Histology Core.

Slides were washed twice and blocked for 1 hour in blocking buffer (5% goat serum, 0.5% BSA, 0.3% Triton X-100, 0.01% azide in PBS). Primary antibodies were added (monoclonal rat anti-mouse Ki-67 antigen, clone TEC-3 [1:50], monoclonal mouse anti-vimentin, clone LN-6 [1:200], used for mKi-67 costaining, polyclonal rabbit anti-mouse FAP [1:1000], monoclonal mouse anti-human smooth muscle actin, clone 1A4 [1:100], polyclonal rabbit anti-mouse vimentin [1:50, used for αSMA costaining], monoclonal mouse anti-human desmin [1:1000], polyclonal rabbit anti-NG2 chondroitin sulfate proteoglycan [1:500], polyclonal rat anti-mouse CD31, clone MEC 13.3 [1:500]). All primary antibodies were incubated for 30–60 minutes at room temperature on 4 μM sections. Sections stained with mouse-derived antibodies were additionally blocked with AffiniPure Fab Fragment Goat Anti-Mouse IgG (H+L) (Jackson ImmunoResearch Laboratories, West Grove, PA) after initial blocking step and prior to staining with primary antibody. Slides were then washed six times in 0.1% Triton X-100 in PBS for 15–30 minutes. Secondary antibodies were added (Alexa Fluor 488 Goat anti-Rat IgG [1:500], Alexa Fluor 568 Goat anti-Mouse IgG [1:500], Alexa Fluor 488 Goat anti-Rabbit [1:400], Alexa Fluor 546 Goat anti-Rabbit [1:500]). All secondary antibodies were added for 1 hour at room temperature. Slides were washed three times in 0.1% Triton X-100 for 15–30 minutes followed by a single wash in PBS for 15–30 minutes and then fixed in 10% formalin.

TUNEL staining was performed using the DeadEnd Fluorometric TUNEL System (Promega) per manufacturer's instructions. Positive controls were treated with DNase I (Ambion, Austin, TX) for 10 minutes followed by three washes with PBS for 5 minutes. Terminal deoxynucleotidyl transferase enzyme was omitted for negative controls. Images of slides were taken using a Nikon (Melville, NY) Eclipse Ti fluorescent scope equipped with a Nikon DS-Qi1Mc camera and NIS-Elements AR3.0 imaging software. Image analysis and background subtraction were performed using NIH ImageJ software.

Determination of Plasma Levels of FAP Prodrugs

Calibration standards consisted of FAP prodrugs, 12ADT, and thapsigargin analogs A12ADT, E12ADT, or S12ADT spiked into mouse plasma along with an internal standard (IS). The internal standard was added to plasma samples from treated mice, and then samples were deproteinated with acetonitrile/0.1% formic acid and resulting supernatants analyzed by liquid chromatography coupled to a quadripole mass spectrometer (LC/MS/MS [PE Sciex API 3000]) according to previously described methods (36). Detection was carried out in positive mode. The turbo ion spray nebulizer settings included nebulizer gas set at 10 mL/min and an ion spray potential of 5500 V. The drying gas temperature was set at 450°C, and its flow was 800 mL/min. A multistep gradient elution HPLC method was

used to separate the prodrugs from the free A12ADT or S12ADT and internal standard with a mobile phase composed of 5% acetonitrile/water/0.1% formic acid (solvent A) and 100% acetonitrile/0.1% formic acid (solvent B), and its initial conditions were 60% solvent A/40% solvent B at a flow rate of 0.25 mL/min. The injection volume was 10 µL, and the separation was carried out in a 100 × 2 mm, 2.5-µm reversed phase column (Phenomenex Luna part number 00D-4446-B0; Torrance, CA). At 1 minute following injection, a linear gradient raised the mobile phase composition to 100% solvent B by 7 minutes with a return to initial conditions at 9 minutes. Calibration was done using standards added to and then extracted from mouse plasma in a range of 0.001–10 µM. Linear regression analysis was used to generate best-fit lines from which peak areas of samples were converted to concentration of prodrug. The terminal half-life ($t_{1/2}$) was determined from the terminal slope (ke) on a log-linear plot of concentration versus time.

In Vivo Assays: Toxicity and Tumor Xenograft Studies

All animal studies described in this report including mouse care and treatment were performed according to protocols reviewed and approved by and performed in accordance with the guidelines of the Animal Care and Use Committee of the Johns Hopkins University School of Medicine.

To determine maximally tolerated dose for efficacy studies, Balb-C mice (n = 3 per group) (Harlan Laboratories, Indianapolis, IN) received intravenous treatment with increasing doses of FAP prodrugs. The highest dose that produced no death after three consecutive daily intravenous injections was selected as the maximally tolerated dose.

For efficacy studies, suspended tumor cells were placed in a 60% mixture of Matrigel Matrix (BD Biosciences, San Jose, CA) in Hank's buffered salt solution at a concentration of 2.0×10^6 cells per 100 µL of solution. LNCaP cells were then injected into the subcutis overlying the rear flanks of 6-week-old male nude mice (n = 10 per group) (Harlan Laboratories, Indianapolis, IN). MCF-7 cells were injected subcutaneously into 6-week-old female nude mice (n = 9–11 per group per experiment) (Harlan Laboratories) previously implanted subcutaneously with a slow-release estrogen pellet (0.72 mg of 17β-estradiol; Innovative Research of America, Sarasota, FL) in the contralateral flank. All mice used received only one injection of tumor cells and therefore only developed a single tumor per mouse with successful implantation. Weekly tumor measurements were made with calipers, and the tumor volume (in cm^3) was calculated by the formula $0.5236 \times L \times W \times H$. The mice were euthanized by CO_2 overdose, and the tumors were weighed and processed for histochemical analysis as previously described (31).

Fractionation of Tumors into Stromal/Epithelial Populations

Subcutaneous tumors (one per mouse from three mice) were harvested from euthanized mice immediately following CO_2 asphyxiation according to IACUC protocols. Tumors were cut into small 1–2-mm pieces followed by digestion in a 0.28% Collagenase I (Sigma), 1% DNAse I (Sigma) solution of RPMI 1640 supplemented with 10% FBS, and 1% antibiotic/antimycotic (Sigma) for 4 hours at 37°C in a shaking incubator. The digested tumor suspension was centrifuged at 1200 rpm for 5 minutes and washed with PBS. The pellet was incubated for 30 minutes at room temperature in a 1 mM DTT (Sigma) solution, washed, and incubated for an additional 30 minutes at room temperature in 0.5% trypsin/EDTA. Trypsin was neutralized with FBS-supplemented RPMI 1640 followed by washes with RPMI 1640 + 10% FBS (once) and PBS (twice). Cells were counted on a Coulter (Beckman-Coulter, Brea, CA) counter.

The cell pellet was resuspended in a PBS buffer (pH 7.2) containing 0.5% BSA and 2 mM EDTA (Miltenyi, Cologne, Germany). FcR blocking reagent (mouse, Miltenyi, Cologne, Germany) and microbeads coated with mouse anti-human epithelial cell adhesion molecule (EpCAM [ie, CD326] antibodies) (Miltenyi, Auburn, CA) were added to the cell suspension and incubated at 4°C for 30 minutes while mixing. Following washing, the cell suspension was magnetically separated using an equilibrated MACS 25 LD Column (Miltenyi). Unlabeled stromal cells were collected in the flow-through and wash fractions. The negatively selected stromal fraction was counted and determined to be approximately 10–15% of the total tumor cell population. The EpCAM-positive epithelial fraction was collected by removing the column from the magnet and flushing with buffer. Enrichment of stromal and epithelial fractions was confirmed by western blotting using antibodies to vimentin (R28, Cell Signaling) and cytokeratin 8 (Santa Cruz Biotechnology) (data not shown). Cell fractions were analyzed for the presence of both pro- and active forms of the drugs by LCMS using a method similar to that described above for the determination of plasma levels. Active drug concentrations were normalized to the cell number in each fraction.

Statistical Analysis

P values were calculated using permutation tests based on 50 000 permutations. For the experiments that had replicate measurements, mixed effects models were used to take into account the correlations of the multiple measures. The models included the indicator of treatment group as a fixed classification factor, and the variance-covariance structure was modeled by assuming the replicate measures from the same sample to be symmetrically correlated while assuming independence of observations from different samples. All statistical tests were two-sided, and *P* values less than .05 were considered statistically significant. All error bars in the figures represent 95% confidence intervals. The analyses were performed using statistical software SAS version 9.3 (SAS Institute, Cary, NC).

Results

Characterization of FAP-Activated Thapsigargin Prodrugs In Vitro

Fibroblasts are relatively resistant to chemotherapy, in part because of a low proliferative index (37–39). Therefore, we selected thapsigargin (TG), a highly toxic natural plant product, as the cytotoxic agent for this strategy (Figure 1, A), because TG-induced apoptosis has previously been shown to be proliferation-independent; thus, TG is equally cytotoxic to both rapidly and slowly proliferating cells (31). TG is a potent inhibitor of the sarcoplasmic/endoplasmic reticulum calcium ATPase (SERCA) pump, a critical intracellular housekeeping protein (40). SERCA pump inhibition results in sustained elevation of intracellular calcium levels, which

Table 1. Effect of amino acid-containing analogs of thapsigargin on different cell lines*

Cell line	Source	IC_{50}, mean nM (95% CI)
MCF-7	Breast cancer	2.9 (2.89 to 2.91)†
LNCaP	Prostate cancer	3.3 (3.22 to 3.38)‡
TSU	Bladder cancer	28.0 (27.88 to 28.12)‡
WPMY-1	Fibroblast	13.3 (10.0 to 16.6)†
CAS-23§	Fibroblast	80.1 (75.0 to 85.2)†
NAS-23§	Fibroblast	76.8 (69.9 to 83.7)†

* Amino acid-containing analogs of thapsigargin, like the parent compound, are highly potent but nonspecific cytotoxic agents that can kill a variety of cell types, including malignant epithelial cells and fibroblasts, in the exponential growth phase. IC_{50} = concentrations that inhibited growth by 50%.
† MTT cell proliferation assay. MTT = 3-(4,5-dimethylthiazol-2-yl)-2,5-diphenyltetrazolium bromide, a yellow tetrazolium salt.
‡ Clonal survival assay.
§ Primary stromal cultures from human prostate cancer specimen (CAS-23) and normal prostate (NAS-23).

triggers apoptosis (41–43). TG is an extremely potent, but non–cell type-specific, cytotoxic agent because normal SERCA pump function is essential for the viability of all cell types (42,44–46). Thus, TG is equipotent in vitro against human cancer cell lines, fibroblasts, endothelial cells, and osteoblasts (31).

As expected for an agent that kills proliferatively quiescent cells, TG is highly toxic in vivo with an LD_{100} of 0.2 mg/kg (31). To exploit the nonspecific cytotoxicity of TG for therapeutic benefit, a FAP-activated prodrug strategy was developed in which a cytotoxic TG analog was coupled to FAP-selective peptide substrates to create inactive prodrugs that only become activated upon release of the peptide from the TG analog by FAP proteolysis. Using an iterative screening approach, we previously identified a series of amino acid–containing TG analogs consisting of 8-*O*-(12-aminododecanoyl)-8-*O*-debutanoyl-thapsigargin (12ADT) (Figure 1, A) coupled to an amino acid that could be readily coupled via a peptide bond to FAP peptide substrates (Figure 1, B) (47). Like TG and 12ADT, these amino acid analogs are potent nonspecific cytotoxins that kill human cancer cells and normal fibroblasts at low nanomolar concentrations (Table 1). In addition, these analogs are equally toxic to both exponentially growing (Table 1) and nonproliferating confluent cultures of fibroblasts (Figure 1, C), as demonstrated by the approximately equimolar potency against the prostatic fibroblast cell line WPMY-1 under these conditions (proliferating cells: mean = 13.3 nM, 95% CI = 11.6 to 15 nM; nonproliferating cells: mean = 24.0 nM, 95% CI = 21.6 to 26.4 nM). The peptide component of each prodrug was selected from a previously generated map of FAP cleavage sites within recombinant human collagen I-derived gelatin (17). The peptide sequences were selected based upon kinetic parameters of FAP hydrolysis (Figure 1, D). TG is poorly soluble in aqueous media at concentrations above 15 μM; therefore, addition of the peptide also enhances solubility of the TG analog more than 1000-fold (ie, prodrugs soluble up to 30 mM).

The FAP-activated prodrugs (ASGPAGP-A12ADT, DSGETGP-A12ADT, and ERGETGP-S12ADT) were cleaved by recombinant FAP to release the active drug (A12ADT or S12ADT) (Figure 1, E). In addition, two non-FAP cleavable controls were generated, a scrambled analog (PETGRSG-E12ADT) and an analog in which the P1-Pro at the FAP-cleavage site is converted to the D-Pro isomer (ERGETGp-S12ADT). FAP was unable to hydrolyze either of these control prodrugs to release the active forms of these drugs (E12ADT or S12ADT, respectively) (Figure 1, E).

Because the prodrugs will be administered systemically via the blood, it is critical to the success of the strategy that the peptide carrier prevents nonspecific cellular uptake of the TG analog in the absence of FAP hydrolysis. To demonstrate this property, we took advantage of the ability of TG and its analogs, via inhibition of the SERCA pump, to produce an acute elevation in intracellular calcium (40,43). Exposure of human TSU bladder cancer cells loaded with the calcium-responsive dye Fura-2 to 50 nM S12ADT or A12ADT generated a rapid rise in intracellular $[Ca^{2+}]$ to several hundred nanomolar levels within minutes of exposure (S12ADT: mean = 202 nM, 95% CI = 145 to 259 nM; A12ADT: mean = 306 nM, 95% CI = 274 to 338 nM). In contrast, because of the inability to penetrate the cell membrane, the noncleaved prodrugs were unable to induce a rise in intracelluar $[Ca^{2+}]$ (vehicle: mean = 98 nM, 95% CI = 66 to 130 nM; ASGPAGP-A12ADT: mean = 102 nM, 95% CI = 79 to 125 nM; DSGETGP-A12ADT: mean = 120 nM, 95% CI = 65 to 175 nM; ERGETGP-S12ADT: mean = 119 nM, 95% CI = 96 to 142 nM; ERGETGp-S12ADT: mean =116 nM, 95% CI = 51 to 181 nM) at concentrations that are approximately 20-fold higher (1 μM, Figure 1, F).

In Vitro Activity of FAP Prodrugs

A soluble, extracellular form of FAP has previously been identified in bovine serum (48), and we observed similar FAP-like activity to be present in 10% FBS containing medium (Figure 2, A). Thus, we took advantage of the FAP-like activity present in FBS-supplemented medium to study the activation of the prodrugs. We determined that all three FAP-activated prodrugs were hydrolyzed in FBS-supplemented medium but not in serum-free medium (Figure 2, 2A). Consistent with FAP as the activating enzyme, neither the scrambled nor the D-Pro isomer were hydrolyzed in this medium (Figure 2, A). Subsequently, to test whether cytotoxic levels of the active TG analog could be released under these conditions, the prodrugs were added to the medium and incubated with MCF-7 breast cancer cells to determine their potency in vitro. MCF-7 cell growth was inhibited by 50% at a mean concentration of approximately 3.5 nM by the FAP-activated prodrugs. In contrast, both the scrambled and D-isomer analogs (non-FAP cleavable) were at least 300-fold less potent with $IC_{50} > 1$ μM (Figure 2, B).

The presence of FAP-like activity in FBS is not an isolated phenomenon. Previously, Lee et al. (49,50) demonstrated measurable FAP activity in human plasma. This observation led us to investigate whether FAP-like activity was present in the plasma of other species (Figure 2, C), particularly in mouse plasma prior to evaluation of efficacy in mouse models in vivo. Hydrolysis of a FAP-selective fluorescence-quenched peptide in the plasma/serum demonstrated that there is significantly greater FAP-like activity in the mouse relative to the other species tested. This hydrolysis was abrogated by a FAP-selective inhibitor, acetylated-gly-boroPro (AcGbP) (29). The activity in the mouse was up to 10-fold higher than the lowest levels of activity that were observed in human plasma and serum (Figure 2, C).

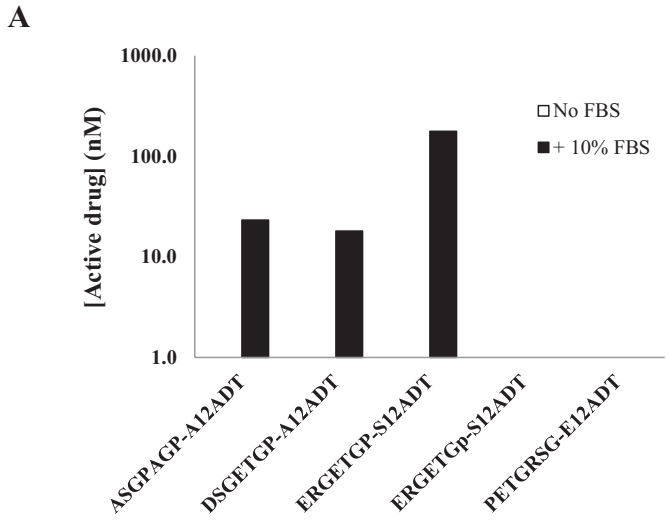

B

	Compound	IC_{50} nM (95% CI)
Active drug	12ADT	2.8 (2.33 to 3.27)
	A12ADT	2.9 (2.8 to 3.0)
	S12ADT	3.5 (3.25 to 3.75)
	E12ADT	1.9 (1.47 to 2.33)
Prodrug	ASGPAGP-A12ADT	3.5 (3.42 to 3.58)
	DSGETGP-A12ADT	3.4 (3.18 to 3.62)
	ERGETGP-S12ADT	3.4 (3.13 to 3.67)
	ERGETGp-S12ADT	>1000
	PETGRSG-E12ADT	>1000

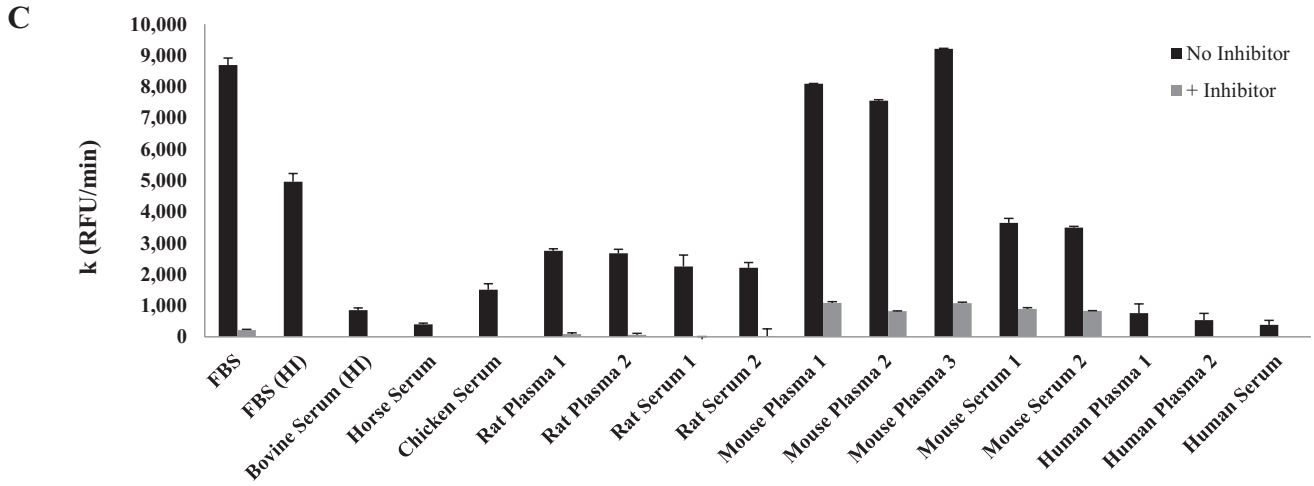

Figure 2. In vitro activity of FAP-activated prodrugs. **A**) Hydrolysis of FAP-activated prodrugs in tissue culture media supplemented with 10% FBS but not in its absence. Non-FAP cleavable prodrug analogs are stable in FBS-supplemented media. **B**) Effect of FAP prodrugs on the growth of the MCF-7 human breast cancer cell line in vitro. Mean absorbance was calculated from a single experiment with seven replicates/concentration and reported with 95% confidence intervals (CI). **C**) Comparison of FAP enzymatic activity in the plasma/serum from multiple species based upon the rate of hydrolysis of a FAP-selective fluorescent substrate (MCa-ASGPAGPA-Dnp, 20 μM). The mouse had as much as 10-fold greater FAP activity in the plasma than did the human. The FAP-selective dipeptide boronic acid inhibitor, AcGbP, was used at a concentration of 200 μM. **Error bars** represent 95% CI. IC_{50} = half maximal inhibitory concentration; FBS = fetal bovine serum; CI = confidence interval; FAP = fibroblast activation protein α; RFU = relative fluorescence units.

The Murine Stroma-Supported Human Cancer Xenograft as a Model for FAP-Activated Prodrug Chemotherapy

The tumor-associated stroma comprises a much lower percentage of the overall tumor mass in mouse xenograft models compared with human primary tumors. In support of earlier studies (41), using the MCF-7 human breast cancer xenograft model, we determined that mouse stromal cells that infiltrate human cancer xenografts also express the mouse homolog of FAP (Figure 3, A), which shares 89% sequence homology with human FAP (41). Like human CAFs, the FAP-expressing mouse stroma acquires a reactive phenotype as indicated by increased expression of α-smooth muscle actin (αSMA) (Figure 3, A). Additionally, homogenates of MCF-7 xenografts can cleave a FAP-selective fluorescence-quenched peptide substrate (Figure 3, B). Although considered "activated," these stromal cells have a low proliferative rate as determined by staining with an anti-mouse Ki-67-specific antibody (Figure 3, C). This proliferative rate is markedly lower than that of the human malignant epithelial cells within the xenograft (Figure 3, C). Overall, these results support the use of mouse tumor xenograft models as a representative system for testing the safety and efficacy of FAP-activated prodrugs.

Immunohistochemical Analysis of FAP Prodrug Effects on the Tumor Stroma

FAP-specific release of the highly lipophilic TG analog from the peptide carrier by FAP-positive CAFs should primarily affect the cells within the stromal compartment rather than the malignant epithelial cells. To assess this effect, MCF-7 xenografts harvested from prodrug-treated mice underwent TUNEL staining to determine apoptotic cell distribution. As hypothesized, the majority of TUNEL-positive nuclei in cells from the ASGPAGP-A12ADT prodrug-treated xenografts were observed in the FAP-expressing tumor stroma (Figure 4, A). A similar overlap in TUNEL positivity

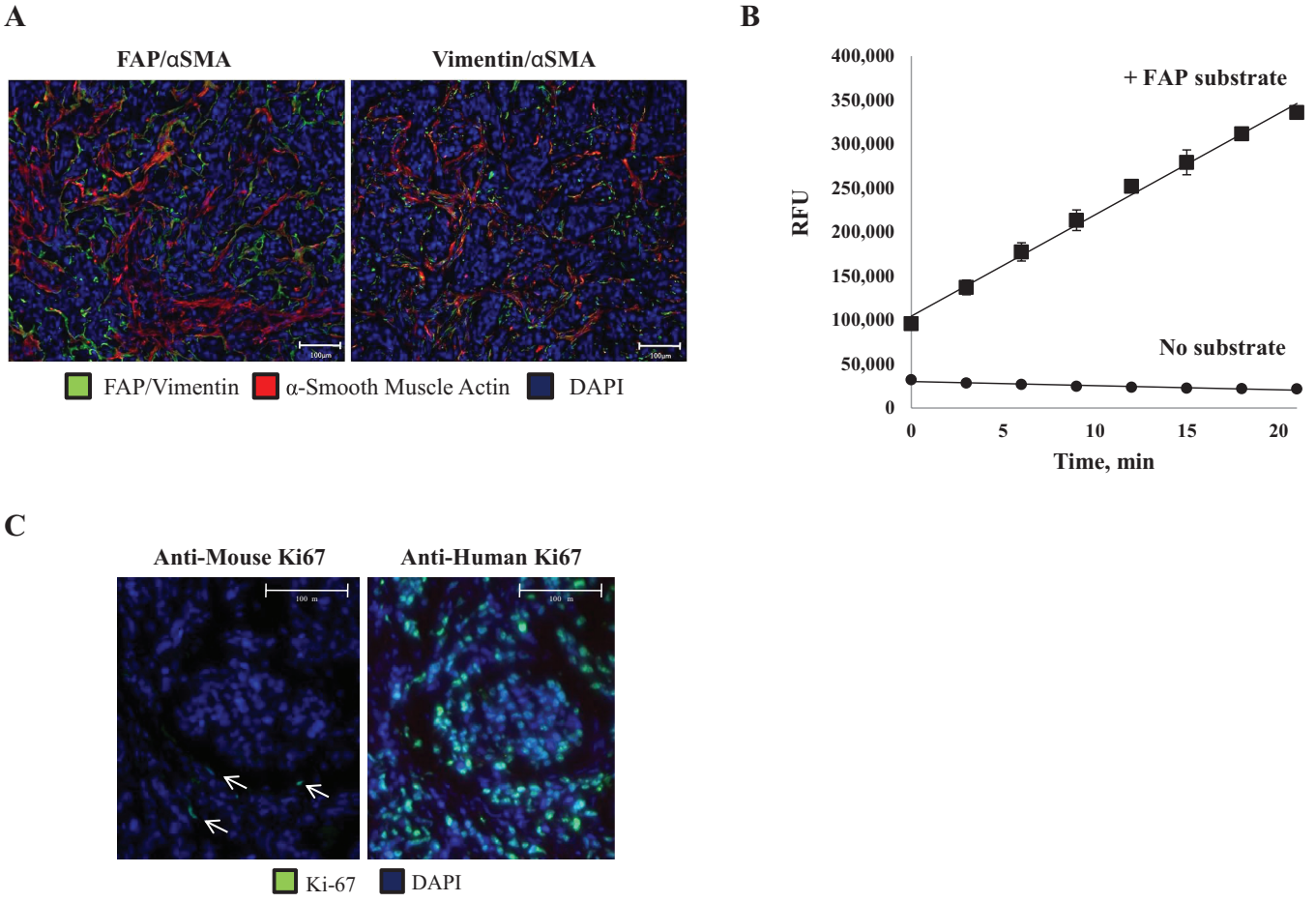

Figure 3. The murine stroma and human cancer xenografts as a model to evaluate FAP-activated prodrugs. **A**) Fibroblasts infiltrating MCF-7 xenografts take on a reactive phenotype as characterized by the coexpression of FAP (left panel) or vimentin (right panel) (**green**) and α-smooth muscle actin (**red**). Images are representative and were taken at ×20 magnification. Scale bars = 100 μm. **B**) Presence of FAP enzymatic activity in MCF-7 tumor homogenates as indicated by the hydrolysis of a FAP-selective fluorescence-quenched peptide substrate (MCa-DRGETGPA-Dnp [1 μM]). **Error bars** represent 95% CI. **C**) Mouse stromal cells have a substantially lower proliferative index (**arrows**, left panel) than do the malignant epithelial cells (right panel) within the xenograft. Tumor sections were stained using an anti-mouse (left panel) or anti-human (right panel) Ki-67-specific antibody (**green**). The nuclei are counterstained with DAPI (**blue**). Image is representative and was taken at ×20 magnification. Scale bars = 100 μm. FAP = fibroblast activation protein α; RFU = relative fluorescence units; SMA = smooth muscle actin; DAPI = 4′,6-diamidino-2-phenylindole; CI = confidence intervals.

and αSMA staining was also observed (Figure 4, B). Quantitatively, there were approximately 90% more TUNEL-positive nuclei in the ASGPAGP-A12ADT prodrug-treated tumors compared with the untreated controls (Figure 4, C). Within these same FAP prodrug-treated tumors, approximately 80% of the total TUNEL-positive cells were in the stroma, whereas only about 40% of the total TUNEL-positive cells were in the stroma of the control tumors (Figure 4, D).

FAP activation of the prodrugs within the tumor stroma microenvironment could potentially produce a "bystander" effect on other stromal cells because of release of the TG analog into the extracellular fluid surrounding both FAP-positive and FAP-negative

Figure 4. Stromal-selective cell death in tumors treated with FAP-activated prodrugs. **A**) FAP-positive stromal cells (**red**) selectively undergo apoptosis as indicated by TUNEL-positive (**green**) nuclei following treatment with a FAP-activated prodrug, ASGPAGP-A12ADT, whereas untreated control tumors show a more general pattern of cell death in MCF-7 xenografts. Nuclei are counterstained with DAPI (**blue**). Images are representative of three images per tumor and three tumors per group. Images were taken at both ×10 and ×20 magnifications. **Scale bars** = 100 μm. **B**) Stromal cells positive for α-smooth muscle actin (**red**) selectively undergo apoptosis as indicated by TUNEL-positive (**green**) nuclei following treatment with a FAP-activated prodrug (ASGPAGP-A12ADT or DSGETGP-A12ADT) compared with untreated control tumors from mice bearing MCF-7 xenografts. Nuclei are counterstained with DAPI (**blue**). Images are representative of three images per tumor and three tumors per group. Images were taken at ×20 magnification. **Scale bars** = 100 μm. **C**)There are approximately 90% more TUNEL-positive cells in tumors treated with a FAP-activated prodrug. Quantitation of images represented in (**A**). Average of 6–9 images per group. **Error bars** represent 95% CI. **Asterisks** indicate statistically significant $P < .05$, determined using mixed effects models. (Note: the analysis was based on each individual replicate, not their mean.) **D**) Approximately 80% of the total apoptotic (TUNEL-positive) cells from the FAP-activated prodrug-treated tumors are of stromal lineage compared with approximately 40% of the total TUNEL-positive cells in the untreated control tumors. Quantitation of images represented in (**C**). Average of nine images per group. **Error bars** represent 95% CI. **Asterisks** indicate statistically significant difference from untreated control, with $P < .05$ determined using mixed effects models (Note: the

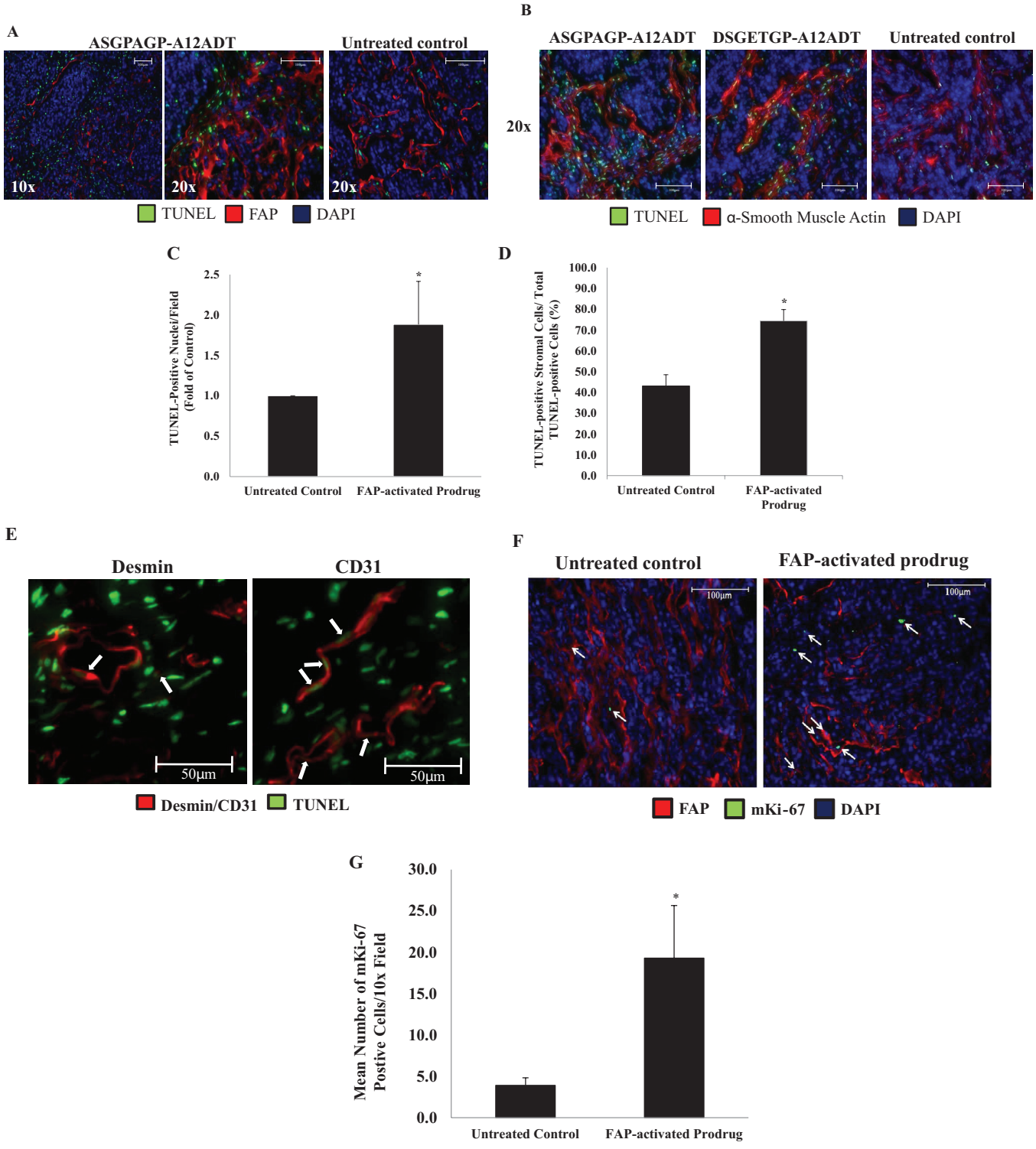

Figure 4 (Continued).

analysis used each individual replicate.) **E**) Treatment of tumors with a FAP-activated prodrug produces a bystander effect resulting in the death of cells adjacent to areas of FAP expression. **White arrows** indicate desmin-positive pericytes (left panel, **red**) and CD31-positive endothelial cells (right panel, **red**) in the stromal compartment undergoing apoptosis (TUNEL-positive, **green**) in FAP-activated prodrug-treated tumors. Nuclei are counterstained with DAPI (**blue**). Images taken at ×40 magnification. **Scale bars** = 50 μm. **F**) Stromal cells within regions of FAP (**red**) expression in xenografts begin to proliferate (**arrows**) following treatment with a FAP-activated prodrug (right panel) compared with those in untreated controls (left panel) as indicated by cells staining positive for an anti-mouse Ki-67-specific antibody (**green**). Nuclei are counterstained with DAPI (**blue**). Images are representative of six images per tumor and three tumors per group. Both images were taken at ×10 magnification. **G**) There is approximately fivefold greater proliferation of mouse stromal cells in MCF-7 xenografts treated with a FAP-activated prodrug. Quantitation of images represented in (**F**). Average of nine images per group. **Error bars** represent 95% CI. **Asterisks** indicate statistically significant difference from untreated control, with $P < .05$, determined using mixed effects models (Note: the analysis used each individual replicate.) TUNEL = terminal deoxynucleotidyl transferase dUTP nick end labeling; FAP = fibroblast activation protein α; RFU = relative fluorescence units; DAPI = 4′,6-diamidino-2-phenylindole; CI = confidence interval.

cells. To assess this bystander effect, xenografts were costained for TUNEL positivity in combination with stains for desmin to demarcate pericytes and CD31 to indicate endothelial cells. In both cases, desmin-positive pericytes and CD31-positive endothelial cells with TUNEL-positive nuclei were observed in tumors treated with a FAP-activated prodrug (ASGPAGP-A12ADT) (Figure 4, E). These immunohistochemistry results demonstrate increased TUNEL-positive cells consistent with the induction of apoptosis within the tumor stroma. However, within this compartment, the level of staining for FAP and αSMA did not appear to decrease (Figure 4, A). These results suggest that the stromal compartment becomes repopulated because of either proliferation of remaining local cells or the invasion of mesenchymal stem cells to replenish the pool of FAP-expressing cells. To evaluate this question, we utilized a mouse-specific Ki-67 monoclonal antibody to determine the effects of the FAP prodrugs on proliferation within the mouse-derived stroma of human cancer xenografts. These results again demonstrated a remarkably low proliferative index within the stroma of untreated controls (Figure 4, F). However, 24 hours after the last FAP-activated prodrug dose (ASGPAGP-A12ADT), a fivefold increase in stromal cell proliferation was observed (Figure 4, F and G).

Efficacy of FAP-Activated Prodrugs Versus MCF-7 Human Breast Cancer Xenografts

Having demonstrated that the FAP-prodrugs preferentially killed stromal cells compared with malignant epithelial cells, we next performed in vivo efficacy studies to determine if the effect on cells in the stromal compartment was of sufficient magnitude to inhibit overall tumor growth. To perform these efficacy studies, we first needed to determine the maximum tolerated dose for each prodrug. The single dose LD_{100} of the active form of the drug A12ADT was 10 nmoles/dose (ie, approximately 0.3 mg/kg) (Figure 5, A). Treatment with A12ADT at the maximally tolerated dose of approximately 0.03 mg/kg for three consecutive doses produced no effect on MCF-7 xenograft growth (Figure 5, B). In contrast, the single dose LD_{100} for each prodrug was 100-fold higher at 1000 nmoles (approximately 60–70 mg/kg). Subsequently, we determined that three consecutive daily IV injections of 100 nmoles (approximately 6–7 mg/kg) of each of the prodrugs exhibited no significant toxicity in the hosts during an observation period of more than 1 month (Figure 5, A).

On the basis of this survival study, we selected a dosing regimen consisting of three consecutive daily IV injections of each individual prodrug at 100 nmoles/dose. The plasma half-life ($t_{1/2}$) of one of the prodrugs, ASGPAGP-A12ADT, was determined to be approximately 4.5 hours in nude mice (Figure 5, C). In addition, although mouse plasma hydrolyzed FAP substrates in vitro, we observed minimal activation (<0.1%) of the prodrugs in mouse plasma in vivo (Figure 5, C, inset). This apparent discrepancy between in vivo and ex vivo hydrolysis can potentially be attributed to clearance from circulation as a result of the short half-life of these compounds in vivo, in addition to differences in hydrolysis rates and specificity between the FAP-activated prodrug used here and the fluorescence-quenched peptide substrate used in the ex vivo analysis. We observed a statistically significant inhibition of tumor growth compared with untreated controls (mean tumor volume = 0.417 mm^3, 95% CI = 0.342 to 0.492 mm^3) following a single 3-day course of the FAP-activated prodrugs, ASGPAGP-A12ADT (mean tumor volume = 0.247 mm^3, 95% CI = 0.205 to 0.289 mm^3), and DSGETGP-A12ADT (mean tumor volume = 0.195 mm^3, 95% CI = 0.133 to 0.257 mm^3) (Figure 5, D).

To confirm that the antitumor effect was due to FAP activation, a separate study was performed to compare the effect of two 3-day cycles of the ASGPAGP-A12ADT prodrug to the scrambled and D-isomer prodrugs (Figure 5, E). In this study, only the FAP-activated prodrug (ASGPAGP-A12ADT) produced a measurable antitumor effect with a maximal treated-to-control tumor volume ratio of .36 (treated: mean = 0.206 mm^3, 95% CI = 0.068 to 0.344 mm^3; control: mean = 0.580 mm^3, 95% CI = 0.267 to 0.893 mm^3) at day 21 after therapy. No statistically significant effect on body weight was observed in the prodrug-treated groups compared with the untreated controls in these studies (Figure 5, F).

Consistent with the immunohistochemical studies demonstrating stromal selective death, we harvested MCF-7 tumors and used an EpCAM-based magnetic bead strategy to separate cells from

Figure 5. Therapeutic index and efficacy of FAP-activated prodrugs versus MCF-7 breast cancer xenografts in vivo. **A**) Maximum tolerated dose (MTD) of FAP prodrugs in Balb-C mice (n = 3 per group). The MTD of the FAP prodrugs was 100-fold higher than that of the active drug without the peptide carrier. The number of mice surviving each dosing level is listed as a fraction of the total number of mice dosed at that level. The number of consecutive daily doses given at each level is listed in parentheses. **B**) Mice (nine per group) treated with A12ADT intravenously (IV) at the MTD (approximately 0.3 mg/kg) for three consecutive doses had no effect on the growth of MCF-7 xenografts compared with vehicle controls. **Error bars** represent 95% CI. **C**) Half-life ($t_{1/2}$) of ASGPAGP-A12ADT in mouse plasma was determined to be approximately 4.5 hours with no accumulation of the prodrug seen at 24 hours following the second and third doses. Inset shows that activation of the prodrug in mouse plasma in vivo represents less than 0.1% of the total amount given and is cleared rapidly. **D**) Mice bearing MCF-7 xenografts were treated intravenously with a single 3-day course of 100 nmoles/day (approximately 6–7 mg/kg/day) with one of two FAP-activated prodrugs (ASGPAGP-A12ADT or DSGETGP-A12ADT) and compared with untreated control tumors. Graph represents the cumulative mean of four independent experiments with approximately nine mice/group/experiment. **Error bars** represent 95% CI. **Asterisks** indicate statistically significant $P < .05$, determined using permutation test to compare means at each point. **E**) Mice bearing MCF-7 xenografts were treated with either a FAP-activated prodrug (ASGPAGP-A12ADT) or one of two non-FAP cleavable prodrug analogs (PETGRSG-E12ADT or ERGETGp-S12ADT, where "p" represents D-isomer of Pro) and compared with untreated control tumors. Treatment regimen consisted of two intravenous courses of three consecutive daily 100 nmole (~6–7 mg/kg) doses with a 2-week recovery period between cycle initiations. Each group contained 10–11 mice in a single experiment. **Error bars** represent 95% CI. **Asterisks** indicate statistically significant differences from untreated control, with $P < .05$, determined using permutation test to compare means at each point. **F**) Effect of FAP-activated prodrug therapy on the body weight of mice. **Error bars** represent 95% CI. **G**) Active drug accumulation within the stromal compartment of tumors treated with a FAP-activated prodrug. Three animals bearing MCF-7 xenografts were treated with a FAP-activated prodrug, ERGETGP-S12ADT, for a single intravenous 3-day course of 100 nmoles/day (6.8 mg/kg/day). Harvested tumors were digested and fractionated into epithelial and stromal cell populations based upon EpCAM expression. Concentrations of active drug present in these fractions were determined by LCMS, normalized to cell number, and expressed as a ratio (stromal:epithelial). CI = confidence interval; FAP = fibroblast activation protein α.

A

Compound	Surviving fraction (No. of consecutive daily doses)				
	1nmole	10nmoles	100nmoles	300nmoles	1000nmoles
ASGPAGP-A12ADT	--	--	3/3 (3)	3/3 (2) 0/3 (3)	0/3 (1)
DSGETGP-A12ADT	--	--	3/3 (3)	3/3 (2) 0/3 (3)	0/3 (1)
ERGETGP-S12ADT	--	--	3/3 (3)	3/3 (2) 0/3 (3)	0/3 (1)
ERGETGp-S12ADT	--	--	3/3 (3)	3/3 (2) 0/3 (3)	0/3 (1)
PETGRSG-E12ADT	--	--	3/3 (3)	3/3 (2) 0/3 (3)	0/3 (1)
A12ADT	3/3 (3)	0/3 (1)	0/3 (1)	--	--

B

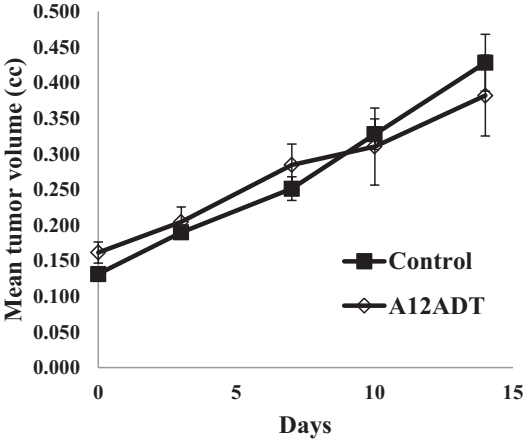

C

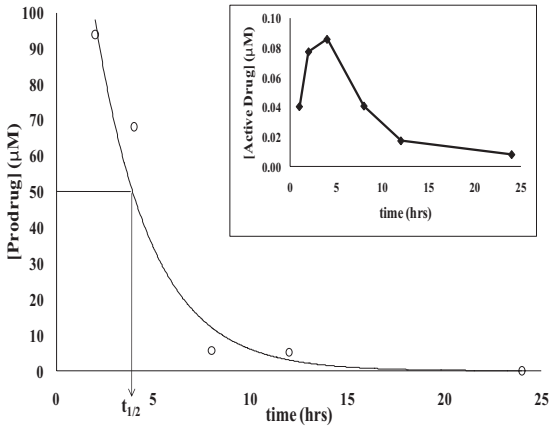

D

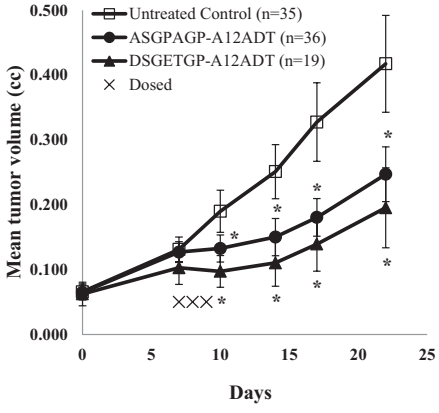

E

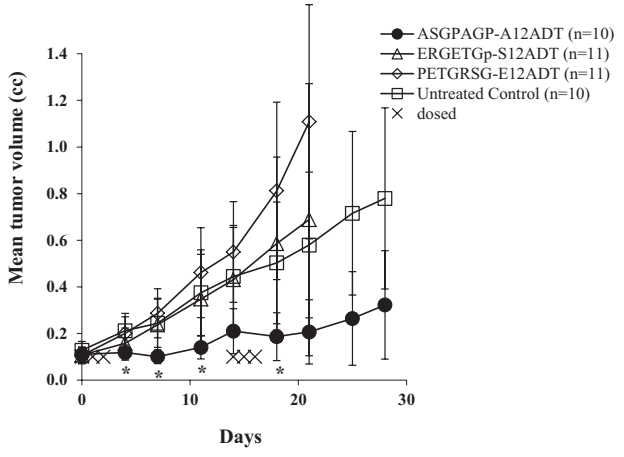

F

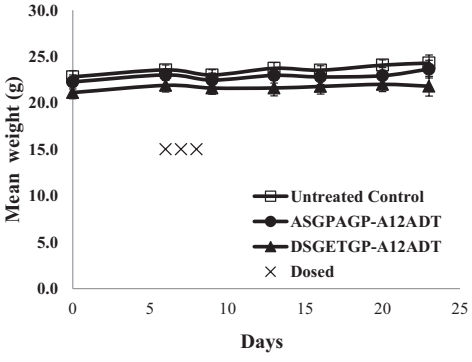

G

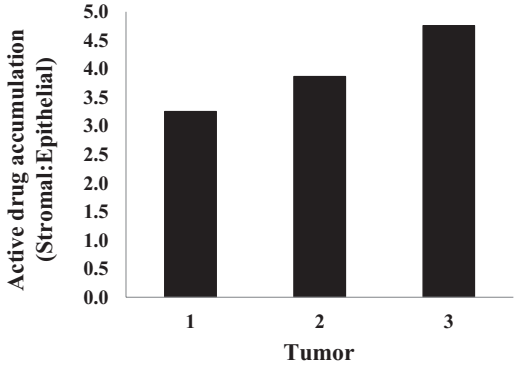

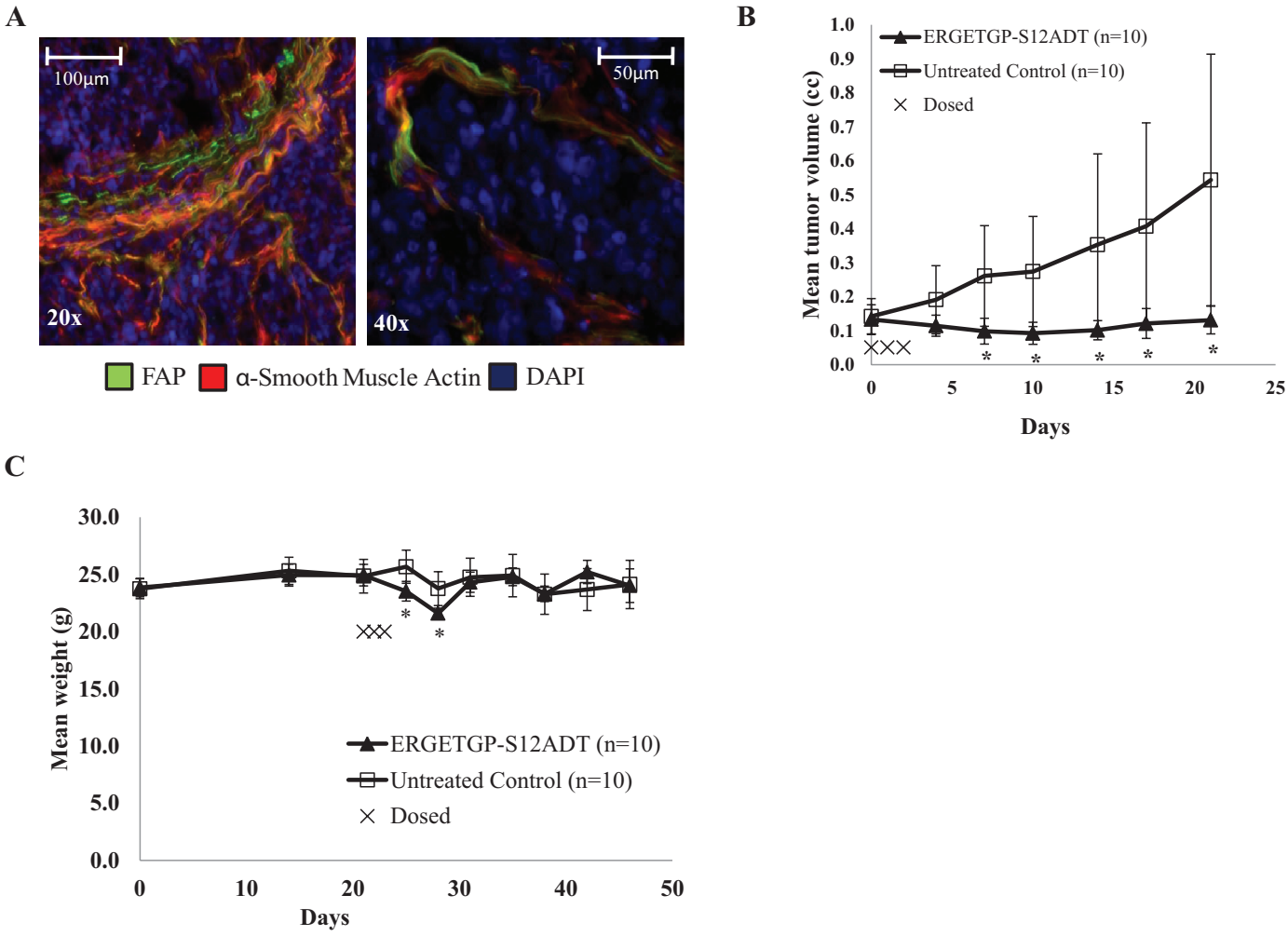

Figure 6. Efficacy of FAP-activated prodrugs versus LNCaP prostate cancer xenografts in vivo. **A**) FAP expression in the stroma of LNCaP human prostate cancer xenografts as indicated by the colocalization of both FAP (**green**) and α-smooth muscle actin (**red**). Nuclei are counterstained with DAPI (**blue**). Images are representative and were taken at ×20 (left panel) and ×40 (right panel) magnification. **Scale bars**: left panel, 100 µm; right panel 50 µm. **B**) Male nude mice (10 per group) bearing LNCaP xenografts were treated intravenously with a single 3-day course of 100 nmoles/day (6.8 mg/kg/day) with a FAP-activated prodrug, ERGETGP-S12ADT, and compared with untreated controls. **Error bars** represent 95% CI. **Asterisks** indicate statistically significant differences from untreated control, with $P < .05$, determined using permutation test to compare means at each point. **C**) Mice bearing LNCaP xenografts (Figure 5, B) treated with the ERGETGP-S12ADT FAP-activated prodrug showed minimal weight loss (<15%) and returned to baseline within 1 week after cessation of therapy. **Error bars** represent 95% CI. **Asterisks** indicate statistically significant differences from untreated control, with $P < .05$, determined using permutation test to compare means at each point. FAP = fibroblast activation protein α; DAPI = 4′, 6-diamidino-2-phenylindole; CI = confidence interval.

the stromal compartment (EpCAM–) from their epithelial neighbors (EpCAM+) within the tumor. Using this methodology, we observed three- to fivefold higher levels of active A12ADT drug within cells of the stromal compartment compared with those in the epithelial cell fraction (Figure 5, G).

Efficacy of FAP-Activated Prodrugs Versus LNCaP Human Prostate Cancer Xenografts

To confirm that the antitumor effect was not confined to a single cancer cell line, we performed additional studies using LNCaP human prostate cancer xenografts. Like the breast cancer model, strong FAP expression was observed in the xenograft stroma, which suggests that FAP expression in the mouse tumor-associated stroma may be a near universal phenomenon, as in human (Figure 6, A). A single 3-day course of the FAP-activated prodrug ERGETGP-S12ADT produced an initial mean tumor regression of 30% for 1 week after treatment followed by sustained growth inhibition that resulted in a maximal treated to control tumor volume ratio of 0.24 (treated: mean = 0.131 mm^3, 95% CI = 0.09 to 0.180 mm^3; control: mean = 0.543 mm^3, 95% CI = 0.173 to 0.913 mm^3) on day 21 after therapy (Figure 6, B). Typical of LNCaP xenograft growth, there is a large degree of variation in the growth of untreated control tumors over time; in contrast, the treated tumors are tightly clustered, demonstrating consistent inhibition of xenograft growth. In this model, the prodrug had a slight effect (ie, <15% decrease) on animal weight at 1 week after dosing, with weight recovering to baseline within an additional week (Figure 6, C).

Discussion

Immunohistochemical analysis confirmed stromal-selective cell death in tumors treated with a FAP-activated prodrug. This stromal selective death produced by these FAP-activated prodrugs was of sufficient magnitude to result in substantial growth inhibition of

human breast and prostate cancer xenografts. These studies demonstrate that the selected FAP-activated prodrugs produce an antitumor effect through selective death of tumor-associated stromal cells without excessive toxicity to the host.

Although surprisingly little is known about FAP's physiological role or substrates, there has been intense investigation into the potential exploitation of FAP as a therapeutic target in the two decades since its discovery (11,29,51–57). This attention derives from FAP's relatively restricted expression within the reactive stroma associated with as many as 90% of all solid malignancies (12,19–21) with no or minimal expression seen in adjacent normal tissue. In contrast, FAP is not observed at high levels in a normal, healthy adult outside areas of wound healing, although it has been implicated in other disease states, such as liver cirrhosis (58), rheumatoid and osteoarthritis (59), bone and soft tissue sarcomas (60), and various fibrogenic disorders (61). The therapeutic strategies explored to date have focused on inhibition of FAP's enzymatic activity using antibody- or small molecule inhibitor-based approaches (29,51–57). These approaches rely on the assumption that FAP expression is protumorigenic. Multiple studies interrogating FAP's role in tumorigenesis have yielded contradictory results relative to tumor growth and survival. FAP has been implicated in tumor promotion through multiple studies demonstrating increases in tumor incidence, growth, and microvessel density using a variety of in vivo models (51,62–64). In contrast, FAP expression decreased tumorigenicity in mouse models of melanoma (65) and was associated with longer survival in patients with invasive ductal carcinoma of the breast (66). These conflicting results suggest that FAP's function may be dependent upon the tissue or exact context of its expression within different tumor microenvironments.

One advantage of this FAP-activated prodrug strategy is that it should have a therapeutic benefit independent of FAP's role in tumor pathophysiology because it relies only upon FAP's presence and unique post-prolyl endopeptidase activity to selectively activate a prodrug in the tumor microenvironment. FAP is a membrane-bound protease whose catalytic site has access to the peritumoral fluid of the tumor microenvironment where it can activate the prodrug. This extracellular activation results in the death of CAFs but also produces a bystander effect as demonstrated by the death of pericytes and endothelial cells within these xenografts. Finally, the selection of a thapsigargin analog as the cytotoxic "payload" is equally important for the success of the strategy because this highly lipophilic agent, upon release from the peptide, rapidly accumulates within nonproliferating stromal cells and induces cell-cycle independent apoptosis. Our hypothesis was that a therapeutic effect could be achieved by exploiting a stromal-restricted protease for activation of a cytotoxic compound within the tumor microenvironment. The hypothesis is supported by data demonstrating that tumor growth is inhibited by FAP-activated prodrug treatment of human cancer xenografts. Furthermore, immunohistochemical staining of tumors treated with a FAP-activated prodrug (ASGPAGP-A12ADT) shows stromal-selective cell death and a bystander effect on pericytes and endothelial cells in areas adjacent to FAP expression. Moreover, fractionation of ASGPAGP-A12ADT prodrug-treated tumors into epithelial and stromal populations reveals a three- to fivefold accumulation of the active drug within the stroma compared with the malignant epithelium. The mechanism underlying this antitumor effect is not known and currently under study. However, the antitumor efficacy may be due to direct cytotoxic effects on the FAP-expressing population (CAFs), a bystander effect targeting the vasculature and epithelial cells, or a combination of effects on primary and secondary targets. Additionally, uptake of the TG analog can profoundly alter protein expression and therefore may affect release of growth and survival signals (67). Finally, Kraman et al. (10) recently demonstrated that selective elimination of FAP-positive stromal cells using a diphtheria toxin receptor transgenic mouse model by itself could produce tumor growth inhibition, which supports our data. Additionally, elimination of FAP-positive stromal cells significantly augmented tumor immunogenicity and regression of murine pancreatic xenografts in mice previously immunized with a mesothelin peptide (10). Although this immune-based mechanism does not explain the antitumor effect we observed because our xenograft experiments were performed in immunocompromised mice that lack T-cell function, it does suggest that combining the FAP prodrug with a vaccine strategy may warrant testing.

Although the results of the current study are encouraging and suggest that a therapeutic effect can be achieved through targeting stromal elements within the tumor, there are limitations. As discussed, we did observe hydrolysis of the peptide substrates in the plasma, suggesting that enzymatically active FAP or a FAP-like activity is present in the circulation or the substrates used are not entirely specific for FAP. Importantly, this activity was far less pronounced in vivo with minimal levels of active drug detected in the circulation. Furthermore, no toxicity was observed in treated animals during the course of the study. In addition, the current study is limited to two xenograft models representing either breast (MCF-7) or prostate (LNCaP) cancer. Therefore, although FAP expression by mouse stromal cells within human cancer xenografts is most likely consistently occurring across xenograft models, these experiments should be repeated with other models to validate the general applicability of this therapeutic strategy to a broad range of solid tumors types, as would be predicted from FAP's expression pattern (12,19–21). Finally, these prodrugs slow tumor growth in these models but do not induce a complete regression, suggesting that combination with other treatment modalities may be necessary to achieve a cure.

In conclusion, these studies validate FAP as a promising target for activating a systemically delivered cytotoxic prodrug within the tumor microenvironment. This study provides evidence that targeting cells within the tumor stroma, independent of the cancer cells themselves, could be a viable strategy for cancer management. Future studies will be directed toward further optimization of this prodrug approach and exploring the effectiveness of a FAP-activated prodrug in combination with other therapeutic modalities, including chemotherapy, radiation, and immune-based therapies.

References

1. Bast R Jr, Kufe DW, Pollock RE, Weichselbaum RR, Holland JF, Frei E III, Gansler TS. *Cancer Medicine*. 5th ed. Hamilton, ON: BC Decker; 2000.
2. Hewitt RE, Powe DG, Carter GI, Turner DR. Desmoplasia and its relevance to colorectal tumour invasion. *Int J Cancer*. 1993;53(1):62–69.
3. Rønnov-Jessen L, Petersen OW, Bissell MJ. Cellular changes involved in conversion of normal to malignant breast: importance of the stromal reaction. *Physiol Rev*. 1996;76(1):69–125.
4. Mueller MM, Fusenig NE. Friends or foes—bipolar effects of the tumour stroma in cancer. *Nat Rev Cancer*. 2004;4(11):839–849.

5. Allinen M, Beroukhim R, Cai L, et al. Molecular characterization of the tumor microenvironment in breast cancer. *Cancer Cell*. 2004;6(1):17–32.
6. Franco OE, Shaw AK, Strand DW, Hayward SW. Cancer associated fibroblasts in cancer pathogenesis. *Semin Cell Dev Biol*. 2010;21(1):33–39.
7. Shimoda M, Mellody KT, Orimo A. Carcinoma-associated fibroblasts are a rate-limiting determinant for tumour progression. *Semin Cell Dev Biol*. 2010;21(1):19–25.
8. Ostman A, Augsten M. Cancer-associated fibroblasts and tumor growth–bystanders turning into key players. *Curr Opin Genet Dev*. 2009;19(1):67–73.
9. Loeffler M, Krüger JA, Niethammer AG, Reisfeld RA. Targeting tumor-associated fibroblasts improves cancer chemotherapy by increasing intratumoral drug uptake. *J Clin Invest*. 2006;116(7):1955–1962.
10. Kraman M, Bambrough PJ, Arnold JN, et al. Suppression of antitumor immunity by stromal cells expressing fibroblast activation protein-alpha. *Science*. 2010;330(6005):827–830.
11. Brennen WN, Isaacs JT, Denmeade SR. Rationale behind targeting fibroblast activation protein-expressing carcinoma-associated fibroblasts as a novel chemotherapeutic strategy. *Mol Cancer Ther*. 2012;11(2):257–266.
12. Garin-Chesa P, Old LJ, Rettig WJ. Cell surface glycoprotein of reactive stromal fibroblasts as a potential antibody target in human epithelial cancers. *Proc Natl Acad Sci USA*. 1990;87(18):7235–7239.
13. O'Brien P, O'Connor BF. Seprase: an overview of an important matrix serine protease. *Biochim Biophys Acta*. 2008;1784(9):1130–1145.
14. Yu DM, Yao TW, Chowdhury S, et al. The dipeptidyl peptidase IV family in cancer and cell biology. *FEBS J*. 2010;277(5):1126–1144.
15. Edosada CY, Quan C, Tran T, et al. Peptide substrate profiling defines fibroblast activation protein as an endopeptidase of strict Gly(2)-Pro(1)-cleaving specificity. *FEBS Lett*. 2006;580(6):1581–1586.
16. Park JE, Lenter MC, Zimmermann RN, Garin-Chesa P, Old LJ, Rettig WJ. Fibroblast activation protein, a dual specificity serine protease expressed in reactive human tumor stromal fibroblasts. *J Biol Chem*. 1999;274(51):36505–36512.
17. Aggarwal S, Brennen WN, Kole TP, et al. Fibroblast activation protein peptide substrates identified from human collagen I derived gelatin cleavage sites. *Biochemistry*. 2008;47(3):1076–1086.
18. Christiansen VJ, Jackson KW, Lee KN, McKee PA. Effect of fibroblast activation protein and alpha2-antiplasmin cleaving enzyme on collagen types I, III, and IV. *Arch Biochem Biophys*. 2007;457(2):177–186.
19. Tuxhorn JA, Ayala GE, Smith MJ, Smith VC, Dang TD, Rowley DR. Reactive stroma in human prostate cancer: induction of myofibroblast phenotype and extracellular matrix remodeling. *Clin Cancer Res*. 2002;8(9):2912–2923.
20. Cohen SJ, Alpaugh RK, Palazzo I, et al. Fibroblast activation protein and its relationship to clinical outcome in pancreatic adenocarcinoma. *Pancreas*. 2008;37(2):154–158.
21. Henry LR, Lee HO, Lee JS, et al. Clinical implications of fibroblast activation protein in patients with colon cancer. *Clin Cancer Res*. 2007;13(6):1736–1741.
22. Bae S, Park CW, Son HK, et al. Fibroblast activation protein alpha identifies mesenchymal stromal cells from human bone marrow. *Br J Haematol*. 2008;142(5):827–830.
23. Scanlan MJ, Raj BK, Calvo B, et al. Molecular cloning of fibroblast activation protein alpha, a member of the serine protease family selectively expressed in stromal fibroblasts of epithelial cancers. *Proc Natl Acad Sci USA*. 1994;91(12):5657–5661.
24. Acharya PS, Zukas A, Chandan V, Katzenstein AL, Puré E. Fibroblast activation protein: a serine protease expressed at the remodeling interface in idiopathic pulmonary fibrosis. *Hum Pathol*. 2006;37(3):352–360.
25. Levy MT, McCaughan GW, Abbott CA, et al. Fibroblast activation protein: a cell surface dipeptidyl peptidase and gelatinase expressed by stellate cells at the tissue remodelling interface in human cirrhosis. *Hepatology*. 1999;29(6):1768–1778.
26. Rettig WJ, Garin-Chesa P, Healey JH, et al. Regulation and heteromeric structure of the fibroblast activation protein in normal and transformed cells of mesenchymal and neuroectodermal origin. *Cancer Res*. 1993;53(14):3327–3335.
27. Campbell I, Polyak K, Haviv I. Clonal mutations in the cancer-associated fibroblasts: the case against genetic coevolution. *Cancer Res*. 2009;69(17):6765–6768; discussion 6769.
28. Puré E. The road to integrative cancer therapies: emergence of a tumor-associated fibroblast protease as a potential therapeutic target in cancer. *Expert Opin Ther Targets*. 2009;13(8):967–973.
29. Edosada CY, Quan C, Wiesmann C, et al. Selective inhibition of fibroblast activation protein protease based on dipeptide substrate specificity. *J Biol Chem*. 2006;281(11):7437–7444.
30. Gibson F, Singh AK, Soumeillant MC, Manchand PS, Humora M, Kronenthal DR. A practical synthesis of l-valyl-pyrrolidine-(2R)-boronic acid: efficient recycling of the costly chiral auxiliary (+)-pinanediol. *Org. Process Res Dev.* 2002;6(6):814–816.
31. Denmeade SR, Jakobsen CM, Janssen S, et al. Prostate-specific antigen-activated thapsigargin prodrug as targeted therapy for prostate cancer. *J Natl Cancer Inst*. 2003;95(13):990–1000.
32. Tombal B, Denmeade SR, Isaacs JT. Assessment and validation of a microinjection method for kinetic analysis of [Ca2+]i in individual cells undergoing apoptosis. *Cell Calcium*. 1999;25(1):19–28.
33. Denmeade SR, Lin XS, Tombal B, Isaacs JT. Inhibition of caspase activity does not prevent the signaling phase of apoptosis in prostate cancer cells. *Prostate*. 1999;39(4):269–279.
34. Mancuso MR, Davis R, Norberg SM, et al. Rapid vascular regrowth in tumors after reversal of VEGF inhibition. *J Clin Invest*. 2006;116(10):2610–2621.
35. Hammers HJ, Verheul HM, Salumbides B, et al. Reversible epithelial to mesenchymal transition and acquired resistance to sunitinib in patients with renal cell carcinoma: evidence from a xenograft study. *Mol Cancer Ther*. 2010;9(6):1525–1535.
36. Janssen S, Rosen DM, Ricklis RM, et al. Pharmacokinetics, biodistribution, and antitumor efficacy of a human glandular kallikrein 2 (hK2)-activated thapsigargin prodrug. *Prostate*. 2006;66(4):358–368.
37. Sivridis E, Giatromanolaki A, Koukourakis MI. Proliferating fibroblasts at the invading tumour edge of colorectal adenocarcinomas are associated with endogenous markers of hypoxia, acidity, and oxidative stress. *J Clin Pathol*. 2005;58(10):1033–1038.
38. Hasebe T, Sasaki S, Sugitoh M, Ono M, Saitoh N, Ochiai A. Proliferative activities of tumor stromal cells play important roles in tumor thickness and progression of T3 ulcerative-type colorectal cancer. *Virchows Arch*. 2003;442(6):569–576.
39. Fox SB, Gatter KC, Bicknell R, et al. Relationship of endothelial cell proliferation to tumor vascularity in human breast cancer. *Cancer Res*. 1993;53(18):4161–4163.
40. Lytton J, Westlin M, Hanley MR. Thapsigargin inhibits the sarcoplasmic or endoplasmic reticulum Ca-ATPase family of calcium pumps. *J Biol Chem*. 1991;266(26):17067–17071.
41. Furuya Y, Lundmo P, Short AD, Gill DL, Isaacs JT. The role of calcium, pH, and cell proliferation in the programmed (apoptotic) death of androgen-independent prostatic cancer cells induced by thapsigargin. *Cancer Res*. 1994;54(23):6167–6175.
42. Denmeade SR, Isaacs JT. The SERCA pump as a therapeutic target: making a "smart bomb" for prostate cancer. *Cancer Biol Ther*. 2005;4(1):14–22.
43. Lin XS, Denmeade SR, Cisek L, Isaacs JT. Mechanism and role of growth arrest in programmed (apoptotic) death of prostatic cancer cells induced by thapsigargin. *Prostate*. 1997;33(3):201–207.
44. Thastrup O, Cullen PJ, Drøbak BK, Hanley MR, Dawson AP. Thapsigargin, a tumor promoter, discharges intracellular Ca2+ stores by specific inhibition of the endoplasmic reticulum Ca2(+)-ATPase. *Proc Natl Acad Sci USA*. 1990;87(7):2466–2470.
45. Sagara Y, Inesi G. Inhibition of the sarcoplasmic reticulum Ca2+ transport ATPase by thapsigargin at subnanomolar concentrations. *J Biol Chem*. 1991;266(21):13503–13506.
46. Davidson GA, Varhol RJ. Kinetics of thapsigargin-Ca(2+)-ATPase (sarcoplasmic reticulum) interaction reveals a two-step binding mechanism and picomolar inhibition. *J Biol Chem*. 1995;270(20):11731–11734.
47. Jakobsen CM, Denmeade SR, Isaacs JT, Gady A, Olsen CE, Christensen SB. Design, synthesis, and pharmacological evaluation of thapsigargin analogues for targeting apoptosis to prostatic cancer cells. *J Med Chem*. 2001;44(26):4696–4703.
48. Collins PJ, McMahon G, O'Brien P, O'Connor B. Purification, identification and characterisation of seprase from bovine serum. *Int J Biochem Cell Biol*. 2004;36(11):2320–2333.

49. Lee KN, Jackson KW, Christiansen VJ, Chung KH, McKee PA. A novel plasma proteinase potentiates alpha2-antiplasmin inhibition of fibrin digestion. *Blood*. 2004;103(10):3783–3788.
50. Lee KN, Jackson KW, Christiansen VJ, Lee CS, Chun JG, McKee PA. Antiplasmin-cleaving enzyme is a soluble form of fibroblast activation protein. *Blood*. 2006;107(4):1397–1404.
51. Santos AM, Jung J, Aziz N, Kissil JL, Puré E. Targeting fibroblast activation protein inhibits tumor stromagenesis and growth in mice. *J Clin Invest*. 2009;119(12):3613–3625.
52. Ostermann E, Garin-Chesa P, Heider KH, et al. Effective immunoconjugate therapy in cancer models targeting a serine protease of tumor fibroblasts. *Clin Cancer Res*. 2008;14(14):4584–4592.
53. Scott AM, Wiseman G, Welt S, et al. A phase I dose-escalation study of sibrotuzumab in patients with advanced or metastatic fibroblast activation protein-positive cancer. *Clin Cancer Res*. 2003;9(5):1639–1647.
54. Eager RM, Cunningham CC, Senzer N, et al. Phase II trial of talabostat and docetaxel in advanced non-small cell lung cancer. *Clin Oncol (R Coll Radiol)*. 2009;21(6):464–472.
55. Hofheinz RD, al-Batran SE, Hartmann F, et al. Stromal antigen targeting by a humanised monoclonal antibody: an early phase II trial of sibrotuzumab in patients with metastatic colorectal cancer. *Onkologie*. 2003;26(1):44–48.
56. Messerschmidt SK, Musyanovych A, Altvater M, et al. Targeted lipid-coated nanoparticles: delivery of tumor necrosis factor-functionalized particles to tumor cells. *J Control Release*. 2009;137(1):69–77.
57. Samel D, Muller D, Gerspach J, et al. Generation of a FasL-based proapoptotic fusion protein devoid of systemic toxicity due to cell-surface antigen-restricted Activation. *J Biol Chem*. 2003;278(34):32077–32082.
58. Wang XM, Yao TW, Nadvi NA, Osborne B, McCaughan GW, Gorrell MD. Fibroblast activation protein and chronic liver disease. *Front Biosci*. 2008;13:3168–3180.
59. Bauer S, Jendro MC, Wadle A, et al. Fibroblast activation protein is expressed by rheumatoid myofibroblast-like synoviocytes. *Arthritis Res Ther*. 2006;8(6):R171.
60. Dohi O, Ohtani H, Hatori M, et al. Histogenesis-specific expression of fibroblast activation protein and dipeptidylpeptidase-IV in human bone and soft tissue tumours. *Histopathology*. 2009;55(4):432–440.
61. Juillerat-Jeanneret L, Gerber-Lemaire S. The prolyl-aminodipeptidases and their inhibitors as therapeutic targets for fibrogenic disorders. *Mini Rev Med Chem*. 2009;9(2):215–226.
62. Cheng JD, Dunbrack RL Jr, Valianou M, Rogatko A, Alpaugh RK, Weiner LM. Promotion of tumor growth by murine fibroblast activation protein, a serine protease, in an animal model. *Cancer Res*. 2002;62(16):4767–4772.
63. Liao D, Luo Y, Markowitz D, Xiang R, Reisfeld RA. Cancer associated fibroblasts promote tumor growth and metastasis by modulating the tumor immune microenvironment in a 4T1 murine breast cancer model. *PLoS ONE*. 2009;4(11):e7965.
64. Huang Y, Wang S, Kelly T. Seprase promotes rapid tumor growth and increased microvessel density in a mouse model of human breast cancer. *Cancer Res*. 2004;64(8):2712–2716.
65. Ramirez-Montagut T, Blachere NE, Sviderskaya EV, et al. FAPalpha, a surface peptidase expressed during wound healing, is a tumor suppressor. *Oncogene*. 2004;23(32):5435–5446.
66. Ariga N, Sato E, Ohuchi N, Nagura H, Ohtani H. Stromal expression of fibroblast activation protein/seprase, a cell membrane serine proteinase and gelatinase, is associated with longer survival in patients with invasive ductal carcinoma of breast. *Int J Cancer*. 2001;95(1):67–72.
67. Vander Griend DJ, Antony L, Dalrymple SL, et al. Amino acid containing thapsigargin analogues deplete androgen receptor protein via synthesis inhibition and induce the death of prostate cancer cells. *Mol Cancer Ther*. 2009;8(5):1340–1349.

Funding

NIH grant (5RO1CA124764) and Susan B Komen Grant (to SRD), NCI Prostate SPORE grant (P50CA58236 to SRD and JTI), and DOD prostate cancer predoctoral mentorship grant (W81XWH-07 to WNB). The funders did not have any involvement in the design of the study; the collection, analysis, and interpretation of the data; the writing of the manuscript; or the decision to submit the manuscript for publication.

Notes

The authors would like to thank the expert assistance and advice of Dr Hans Hammers, George Ndikuyeze, and Stephanie Gerber in the animal perfusion and immunofluorescence studies, as well as Dr Angelo DeMarzo and Jessica Hicks for aid in the immunohistochemistry.

Affiliations of authors: Department of Pharmacology and Molecular Sciences (WNB, SRD) and Department of Oncology, The Sidney Kimmel Comprehensive Cancer Center at Johns Hopkins (DMR, HW, JTI, SRD), The Johns Hopkins University, Baltimore, MD.